


# Combining *in situ* and *ex situ* plankton image data to reconstruct zooplankton (> 1 mm) volume and mass distribution in the global ocean

Yawouvi Dodji Siviadan<sup>1,2,3,\*</sup> , Mathilde Dugenne<sup>1</sup>, Laetitia Drago<sup>1</sup>, Tristan Biard<sup>4</sup>, Emilia Trudnowska<sup>5</sup>, Fabien Lombard<sup>1</sup>, Jean-Baptiste Romagnan<sup>6</sup>, Jean-Louis Jamet<sup>7</sup>, Rainer Kiko<sup>1,8</sup>, Gabriel Gorsky<sup>1</sup> and Lars Stemann<sup>1,9,\*</sup>

<sup>1</sup>Sorbonne Université, CNRS, Laboratoire d'Océanographie de Villefranche, 181 Chemin du Lazaret - 06230 Villefranche-sur-mer, France

<sup>2</sup>Université de Lomé, 01 BP 1515 Lomé (TOGO)

<sup>3</sup>MARBEC, IRD, IFREMER, CNRS, Université de Montpellier, 87 Avenue Jean Monnet, 34200 Sète, France

<sup>4</sup>LOG, Laboratoire d'Océanologie et de Géosciences, Univ. Littoral Côte d'Opale, Univ. Lille, CNRS (Sorbonne Université), UMR 8187, Wimereux, France

<sup>5</sup>Department of Ecology, Institute of Oceanology, Polish Academy of Sciences, Poland

<sup>6</sup>Ifremer Centre Atlantique, Unité Écologie et Modèles pour l'Halieutique (EMH), Nantes, France

<sup>7</sup>Université de Toulon, Aix Marseille Univ., CNRS, IRD, MIO, Toulon, France

<sup>8</sup>Geomar Helmholtz Center for Ocean Research Kiel, Kiel, Germany

<sup>9</sup>Institut Universitaire de France, Paris-France

\*Corresponding authors: dodji.siviadan@imev-mer.fr or syawouvi@yahoo.fr; lars.stemann@imev-mer.fr

Corresponding editor: Marja Koski

## ABSTRACT

Plankton size spectra are important indicators of the ecosystem state, yet such measurements are typically biased by the available sampling methods. Here, we combined individual size measurement from two zooplankton imaging approaches—*in situ* observation by the Underwater Vision Profiler5 and Multinet-collection supplemented by *ex situ* imaging via Zooscan—obtained in the global ocean, to calculate zooplankton normalized biovolume size spectra (NBSS) for all organisms larger than 1 mm. The reconstructed NBSS combining both datasets resulted in increased biomass estimates by adding organisms poorly sampled by either of the methods. The optimal values measured by both methods are used to reconstruct the zooplankton biovolume and biomass distributions. The reconstructed slopes appeared steeper and closer to those measured only by the UVP5 (+7.6%) and flatter than those obtained only from the Multinet (−20%), particularly in tropical and temperate latitudes. The main difference in tropical and temperate NBSS from the two devices is due to the fragile rhizarians that were not accounted for when using net data. When possible, we suggest using *in situ* and *ex situ* technologies together, and we provide potential indications on how to correct for missing components of the community when only one method is available.

**KEYWORDS:** net; Uvp5; zooplankton; Nbss reconstruction; gain; biomass

## INTRODUCTION

Plankton are ubiquitous in the ocean and play important roles in trophic webs and biogeochemical cycles (Longhurst and Glen Harrison, 1989; Turner, 2002, 2015; Steinberg and Landry, 2017; Boyd *et al.*, 2019). In particular, heterotrophic zooplankton are essential drivers of the carbon transfer of primary production to higher trophic layers (Turner, 2004; Frederiksen *et al.*, 2006) or to deep layers where carbon may be sequestered and stored for long periods of time (Cavan *et al.*, 2017; Boyd *et al.*, 2019). The zooplankton size range spans several orders of magnitude from larvae to large jellyfish, with abundances decreasing exponentially with size. This property is encapsulated in the normalized biovolume size spectrum (NBSS hereafter) approach, commonly used by scientists to study plankton and their size distributions. Plankton biovolume can be converted to biomass using taxa-specific allometric relationships (Gorsky *et al.*, 2010; McConville *et al.*, 2016).

Through systematic measurements of organism abundances in increasing biovolume classes, ecologists have shown that the shape of the NBSS varied temporally and spatially depending on the structure of marine ecosystems and could thus be used as an indicator of the productivity and carbon transfer in marine ecosystems (Zhou, 2006; Frangoulis *et al.*, 2010; Petchey and Belgrano, 2010; Gómez-Canchong *et al.*, 2013; Atkinson *et al.*, 2024). Indeed, the intercept of the NBSS can be used as a proxy of the biomass available at the base of the food web (Lombard *et al.*, 2019), while its slope indicates how biomass is transferred across sizes through size-selective feeding, or re-packaging or physical processes (e.g. vertical horizontal entrainments).

Overall, NBSS is a general framework that has been used to quantify plankton distribution on different spatio-temporal scales in order to understand plankton ecology and its contribution to pelagic processes under present and future environmental forcings (Dai *et al.*, 2016; Heneghan *et al.*, 2019;

Ljungström *et al.*, 2020; Hatton *et al.*, 2021; Atkinson *et al.*, 2024). Plankton nets have been the traditional method to collect and study zooplankton in discrete depth layers and locations for almost two centuries, yet a significant fraction of these organisms may be under-sampled with this technique due to their extrusion through the net mesh, entanglement within the net and avoidance and destruction of fragile forms such as gelatinous zooplankton (Bathmann *et al.*, 2001; Gallienne and Robins, 2001; Warren *et al.*, 2001; Remsen *et al.*, 2004). Typically, these methods overlooked the importance of several zooplankton groups, such as rhizarians (Dennett *et al.*, 2002; Remsen *et al.*, 2004; Stemmann *et al.*, 2008; Biard *et al.*, 2016), or gelatinous annelids (Christiansen *et al.*, 2018). The former group includes both mixotroph (most of collodarians and acantharia; Faure *et al.*, 2019) and heterotroph (mostly phaeodaria), which consume similar prey as crustaceans along with marine snow aggregate (Gowing and Wishner, 1992; Gowing and Bentham, 1994). To address these limitations, non-destructive cameras have been developed to identify and quantify the abundance, size and derived biomass of zooplankton *in situ* (Benfield *et al.*, 2007; Picheral *et al.*, 2010, 2022; Stemmann and Boss, 2012; Lombard *et al.*, 2019). While improvements in image quality and artificial intelligence and machine learning are needed for these new camera devices to increase the information on biodiversity and be broadly adopted by zooplankton researchers (Irissou *et al.*, 2022), they provide the increased spatial and temporal resolution needed to study the coupling between physical processes and zooplankton distributions and for modeling zooplankton community structure and trophodynamics (Lombard *et al.*, 2019; Drago *et al.*, 2022; Giering *et al.*, 2022; Soviadan *et al.*, 2022).

In the recent survey by Giering *et al.* (2022), a panel of scientists has recommended a period of overlapping use of *in situ* imaging and physical sampling systems with traditional taxonomy to ensure the continuity and progressive replacement of physical sampling by *in situ* imaging in zooplankton monitoring programs. Studies proposing the comparison of results from nets and imaging cameras at global scale of the open ocean (tropical, temperate and polar systems) in the 0–1000 m water column are rare. This lack of systematic and consistent analysis impairs a global assessment of zooplankton NBSS. The present study uses a combination of observations from Multinet and Underwater Vision Profiler 5 (UVP5) data from 57 stations located in all oceans and five depth layers in the upper kilometer, to reconstruct a complete representation of zooplankton NBSS, and derived biomass, in the equivalent spherical diameter (ESD) > 1 mm size fraction. We then compare these new NBSS estimates to those obtained individually by the net and the UVP5 to discuss the consistent differences and similarities in both the slopes and total biovolume and biomass. We discuss the strengths and limitations of each approach to describe complete zooplankton communities.

## MATERIALS AND METHODS

### Zooplankton sampling and imaging

The Tara Oceans expedition (Karsenti *et al.*, 2011) and Tara Polar Circle took place between 2009 and 2013. Fifty-seven stations (Fig. 1) were sampled with both a Multinet (Roullier

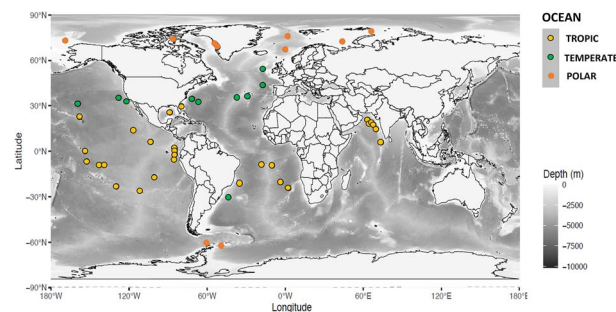


Fig. 1. Location of the 57 stations sampled with UVP5 and Multinet systems, grouped by latitudinal regions: tropic: 0–30°, temperate: 30–60° and polar: > 60°, superimposed on global bathymetry.

*et al.*, 2014; Pesant *et al.*, 2015) and a UVP5 (Picheral *et al.*, 2010). Sampling covered oligotrophic to eutrophic ecosystems. The UVP5 was mounted on the conductivity–temperature–depth Rosette system to record and quantify the size and abundance of specific groups of zooplankton larger than 600  $\mu\text{m}$ . Concurrent measurements of zooplankton size and abundance were thus obtained from these two different approaches. The sampling and processing steps are described in detail below.

The Multinet was composed of five sequential plankton nets with a 300  $\mu\text{m}$  mesh and an aperture of 0.25 m<sup>2</sup>. The Multinet was deployed vertically to sample five discrete depth layers. The Multinet was equipped with a flow meter to estimate the sampled volume, which ranged from 5 to 502 m<sup>3</sup> (median value of 113 m<sup>3</sup>). The five different depth layers were distributed between the surface and 1000 m based on an adaptive strategy depending on observed physical or biological features such as the deep chlorophyll maximum (see rationale in Soviadan *et al.*, 2022) across the 57 global stations. Net samples were preserved in a solution of buffered formaldehyde (4% final concentration). In the laboratory, the samples were rinsed and fractionated with a Motoda box (Motoda, 1959). The final fraction was scanned with the ZooScan system and processed with the Zooprocess software, which allowed a rapid and time-efficient analysis of the plankton samples in a digital format that can be easily stored before further processing (Gorsky *et al.*, 2010).

The *in situ* UVP5 profiles provided automatic information on all particles larger than 100  $\mu\text{m}$  detected by the sensor, in addition to specific information on large zooplankton groups (area > 30 pixels in size, approximately equivalent spherical diameter > 600  $\mu\text{m}$ ) that were large enough to be identified. The UVP5 recorded a maximum of 1 L per frame every 5 cm for a 1 m s<sup>-1</sup> lowering speed, resulting in significantly lower sampled volume compared to the Multinet, ranging from 0.033 to 21.23 m<sup>3</sup> (median value of 4.32 m<sup>3</sup>). Therefore, all profiles of the UVP5 obtained at a given station were pooled (in the case of our study, with ~10 profiles per station) and the counts of all zooplankton were integrated over each depth layer sampled by the nets at the same station. With this data aggregation strategy, the minimum volume integrated over depth and profiles for any given station was > 40 m<sup>3</sup>, providing more robust NBSS estimates that better account for rare organisms in the water column.

The datasets were further grouped in three latitudinal bands (inter-tropical, temperate and polar) and three depth layers (0–200, 200–500, 500–1000 m) to explore NBSS shapes and plankton community compositions across the globe. To balance out the number of stations among the latitudinal bands, we consider the tropical and temperate bands to be larger than their theoretical geographic limits, spanning from 0° to 30°S and N latitude for tropical bands and from 30° to 60° S and N for temperate bands.

In total, the Multinet samples comprised nearly 400 000 images (of which ~53.59% were zooplankton) whereas the UVP5 image collection consisted of 769 297 images (including living and non-living particles), of which 5% were of zooplankton. Both sets of images were uploaded to Ecotaxa (<http://ecotaxa.obs-vlfr.fr>), an online collaborative platform allowing manual validation of the taxonomic classification of each organism predicted with a semi-automatic classifier integrated to the Ecotaxa web application. The images were validated into different groups for each instrument. The high definition of images scanned with the ZooScan allowed identification down to the family (and sometimes to genus), as presented in Soviadan *et al.*, 2022. However, due to the lower definition of the UVP5 images and the smaller cumulative volume, we restricted our NBSS estimates to seven taxonomically coarse categories described in Table I. These have known biovolume to biomass conversion factors (Table I), which were used to compare the absolute and relative contribution of taxon to total biomass for each method.

Once the zooplankton images were validated on Ecotaxa, the concentration and morphometric measurements of each identifiable zooplankton were extracted for every station and net. The biovolume was estimated using the minor and major ellipsoidal axis provided by Zooprocess assuming an ellipsoidal shape (Gorsky *et al.*, 2010). The derived equivalent spherical diameter (ESD) of individual zooplankton varied from 0.25 to 20 mm for the Multinet images and from 0.6 to 20 mm for the UVP5 images. We only considered their overlapping size range and portions where the size spectra were linear ( $ESD > 1$  mm) to compare the two methods.

### Net- and UVP-based plankton size distribution and NBSS estimates

Plankton size distributions were estimated using the broadly-used NBSS approach, which was initially developed for zooplankton (Platt and Denman, 1978). Size distributions were obtained by sorting the individual biovolume of each organism in increasing logarithmically spaced size classes defined by  $[\log(X_n); \log(X_{n+1})]$ , with equal distance:  $\log(X_{n+1}) - \log(X_n) = \log(k)$ , the constant  $k$  is  $2^{1/4}$ . NBSS was calculated by dividing the summed biovolume  $[\sum \text{biovolume} (mm^3)]$  in each size class by the cumulative sampled volume ( $m^3$ ) and further dividing this ratio by the width of each size class interval  $[\Delta \text{biovolume} (mm^3)]$ . In general, all NBSSs present a mode in the size spectrum at the lower size range, reflecting the minimum size of efficient detection and processing by imaging system (see Supplementary Fig. 1), while high variability in the large size range reflects a relatively small sampled volume for that size range (Stemmann and Boss, 2012). In our study, we considered

a maximum of 20 size classes among the 44 initially built for UVP5 imaging devices (Kiko *et al.*, 2022) and that covered both Net and UVP5 zooplankton sizes to calculate the NBSS. Smaller organisms were likely underestimated because of the mesh size or the threshold used to process the raw images; hence, we determined the smallest size class using the approach described by García-Comas *et al.* (2014), which corresponds to the size class where the first maximum NBSS was observed in the net samples (see Supplementary Table I).

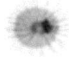
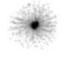
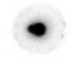

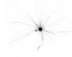









Hereafter, we refer to NBSS estimates derived from zooplankton collected by the Multinet or imaged by the UVP5 as NBSS\_Zmtn and NBSS\_Zuyp, respectively. Using these estimates, we extracted the size spectrum slope which is obtained by simple log-linear regression on the linear part of the size spectrum: 1–8 mm for the NBSS\_Zmtn and the NBSS\_Zuyp.

For biomass estimates, we chose the lower threshold of 1 mm to effectively compare biomass of vignettes validated as zooplankton in this study. This threshold corresponds to the size selected by Barth and Stone (2022) to compare these two methods during 5-day cruises of the Bermuda Atlantic Time-series Study in the Sargasso Sea, or by the size selected by Drago *et al.* (2022) to provide global estimates of zooplankton biomass from UVP5 datasets. The upper threshold was 8 mm and corresponded to the size where NBSS started to flatten due to limited volume observed for rare large organisms.

### Reconstruction of zooplankton NBSS and comparison with the Multinet and the UVP estimates

When comparing the results from the two methods, we assumed that the organisms orientation in the UVP5 images did not significantly bias the observed sizes. To our knowledge, there is no study quantifying this effect. To construct a holistic representation of NBSS estimates, we looked at individual taxonomic group spectra and identified the paired observations where NBSS\_Zmtn and NBSS\_Zuyp were both positive, with the exception of most groups of rhizarians (e.g. Collodaria, Phaeodaria) that presented no positive values in NBSS\_Zmtn (Fig. 2). Therefore, only UVP5-based estimates were used to assess rhizarians NBSS. We note that one group of rhizarians (Other Rhizaria) was detected in several Multinet samples, with sizes below the 1 mm detection limit. However, this group appeared strongly correlated to the UVP5 Foraminifera, with  $ESD > 1$  mm (see Supplementary Fig. 2), suggesting that this group was imaged without their ecoplasmic envelope (pseudopodia) in the Multinet samples and with their ecoplasmic envelope by the UVP5. We thus also used the NBSS\_Zuyp exclusively for this group. Except for rhizarians, we selected the maximum of the non-null paired values (UVP5 and Multinet) within each size class for each taxonomic group and summed the values of the different taxonomic groups to obtain the bulk reconstructed NBSS estimates for all zooplankton. This procedure ensured that the best estimate of each method was used for a specific size and taxonomic group, although we note that over-segmentation (Barth and Stone, 2022), especially with *in situ* datasets, or smaller cumulative volume could result in inflated values that should ideally be discarded. During the annotation, care was taken to identify over-segmented animals

**Table I:** List and examples of images of zooplankton taxa identified in the present study and conversion factors from biovolume to carbon content

Name of the category	Carbon content from volume ( $\mu\text{gC}/\text{mm}^3$ ), median	Typical taxa in the category	Example images from (number of images)	
			UVP5 ( $n = 769\ 297$ )	ZooScan ( $n = 393\ 382$ )
Phaeodaria	(Mansour <i>et al.</i> , 2021) 0.0103	Encompass all rhizarians that were recognized as phaeodarians	 ( $n = 6963$ )	 ( $n = 73$ )
Collodaria	(Mansour <i>et al.</i> , 2021) 0.189	Encompass all rhizarians that were recognized as collodarians	 ( $n = 728$ )	 ( $n = 0$ )
Other Rhizaria	(Mansour <i>et al.</i> , 2021) 0.0103	Encompass all rhizarians, not recognized as collodarians and phaeodarians (e.g. Acantharea Foraminifera)	 ( $n = 6934$ )	 ( $n = 4164$ )
Crustaceans	(McConville <i>et al.</i> , 2016) 0.0892	Encompass all crustaceans (Copepoda, Eumalacostraca, Amphipoda) Copepods being 80% of total count	 ( $n = 19\ 537$ )	 ( $n = 151\ 397$ )
Carnivorous gelatinous	(McConville <i>et al.</i> , 2016) 0.0047	Cnidaria, Ctenophora, Chaetognatha	 ( $n = 1509$ )	 ( $n = 11\ 689$ )
Filter feeders gelatinous	(McConville <i>et al.</i> , 2016) 0.0143	Tunicata	 ( $n = 130$ )	 ( $n = 2094$ )
Other zooplankton	See (Drago <i>et al.</i> , 2022) supplementary 0.0566	Other (Annelida, Hemichordata, Mollusca and other living organisms that are not classified in a particular group)	 ( $n = 3578$ )	 ( $n = 5202$ )

and discard the parts that would have been saved as separate vignettes.

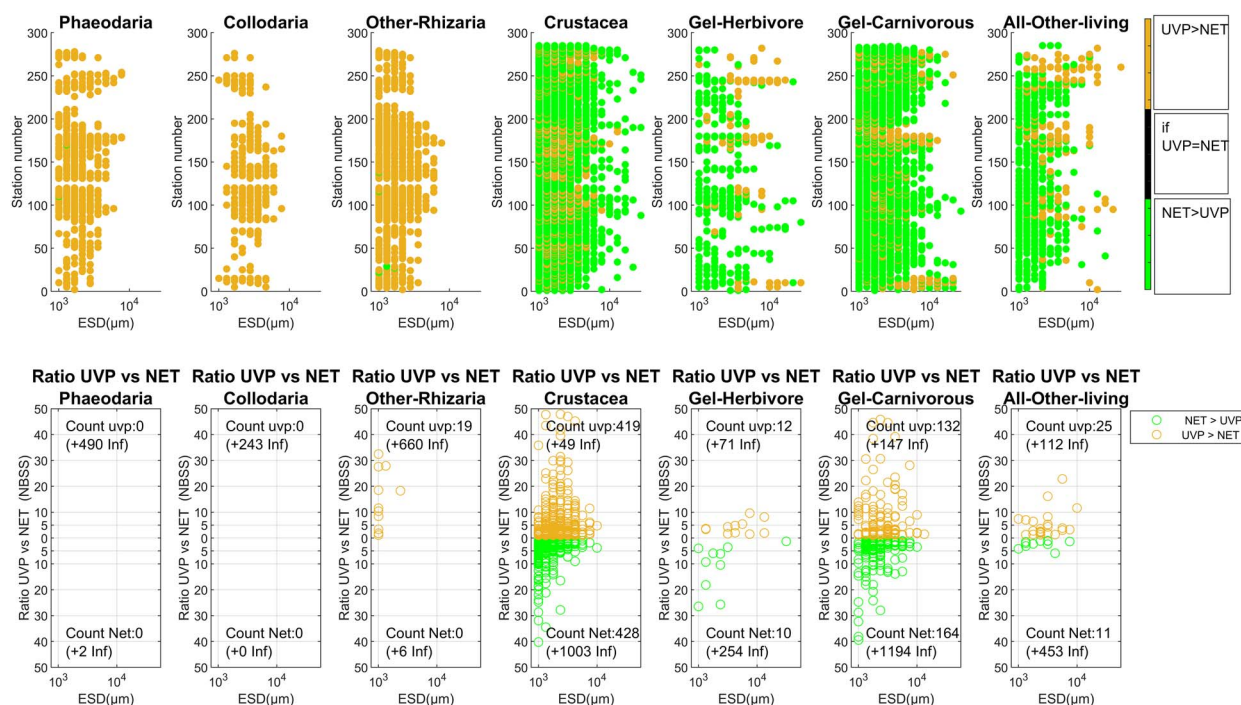
Comparison of the reconstructed NBSS with NBSS\_Zuvp or NBSS\_Zmtn was done by computing the integrated biomass and slopes from all estimates between 1 and 8 mm. We used a non-parametric Kruskal–Wallis test to test for significant differences between slopes and integrated biomass, as well as the Pearson coefficient to test the linear correlations. A compilation of NBSS slopes from previous studies (Dai *et al.*, 2016, 2017) in the epipelagic layer was also used for comparison. The relative gain in biomass or change in slopes (noted  $\partial$ ) were computed using the median values by the following equation:

$$\partial = \frac{Y_{reconstructed} - Y_{measured}}{Y_{measured}} \times 100$$

where  $\partial$  is the % change in NBSS slopes or in the total biomass,  $Y_{reconstructed}$  is the reconstructed value and  $Y_{measured}$  is the observed value from Multinet or UVP only. Absolute offset was calculated as follows:

$$\Delta Y = | Y_{reconstructed} - Y_{measured} |$$

In addition, to explore a potential correction of the reconstructed estimates (NBSS slopes and total biomass) based on the existing sampling strategy (net-collection supplemented by *ex-situ* imaging via Zooscan or *in situ* UVP imaging), we computed the linear regression between the reconstructed values and the measured values when the  $R^2$  is positive and the  $P$ -value  $< 0.05$ .



**Fig. 2.** Illustration of the NBSS selection criteria to build the reconstructed NBSS. The top panel indicates NBSS estimates selection between UVP5 or nets based on the maximum value observed for individual taxonomic groups; the *x*-axis is the size classes in equivalent spherical diameter (ESD,  $\mu\text{m}$ ) calculated from the ellipsoidal biovolume, and the *y*-axis is the order of sampling stations (from deep layers to the surface starting from the first day to the end of the cruise or the selected samples). The bottom panel shows the NBSS ratio of UVP/NET only for the size class when UVP5 and net values are both different from zero. Note that Phaeodaria and Collodaria did not present finite ratio or NBSS estimates from Multinet samples. Gel- means Gelatinous.

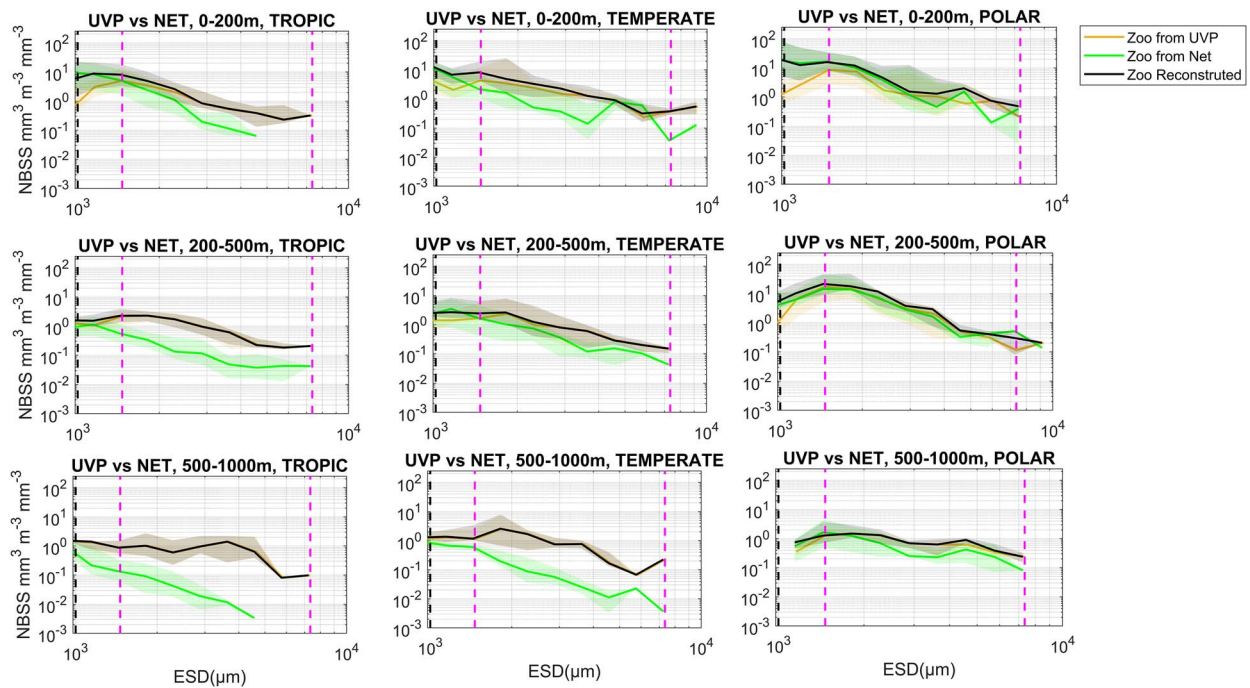
## RESULTS

### Combining taxon-specific observations to reconstruct holistic NBSS estimates

To reconstruct the zooplankton NBSS in the 57 stations, we selected the maximum value observed in all paired NBSS estimates above 1 mm for each individual taxonomic group. The resulting selection is shown in Fig. 2. Collodaria and Phaeodaria were detected almost only in the UVP5 samples. For these groups, we picked UVP5-derived NBSS estimates. A third group, Other-Rhizaria, was detected in both Multinet and UVP5 samples, but with a very distinct size distribution for the two sampling methods (ESD < 1 mm in Multinet samples and ESD > 1 mm in UVP5 samples, see Supplementary Fig. 2a). The total concentration of Other-Rhizaria across all paired samples observations were significantly correlated ( $r^2 = 0.53$ ,  $P\text{-value} = 9.3 \times 10^{-31}$ ,  $y = 0.7x + 0.4$ ), suggesting that they might have been the same organisms (Supplementary Fig. 2b). Crustaceans, mainly copepods, were well detected by the Multinet in small (ESD closer to 1 mm) and large (ESD > 8 mm) size classes, covering a larger size range than the UVP5. However, intermediate size classes (2–8 mm) were generally better sampled with UVP5, with a median ratio (UVP/NET) of 2.77 ( $n = 419$ ), although some samples presented a higher normalized biovolume in Multinet compared to UVP (median: 2.56,  $n = 428$ ). Similarly, gelatinous carnivorous organisms were well detected with the UVP5 at intermediate size classes with a median ratio (UVP/NET) of 4.71 ( $n = 132$ ) against a median ratio NET/UVP of 3.33 ( $n = 164$ ). Gelatinous herbivores and

“Other” zooplankton were mostly found in intermediate size classes by net and in large size classes by UVP5 (Fig. 2). The median ratio of UVP to Multinet normalized biovolume, across all size classes and all taxonomic units, was 3.19 (quartiles of 1.70–9.26) at these locations (Figs 2 and 3).

The median NBSS derived from the UVP5 *in situ* camera (NBSS\_Zuwp) or the Multinet (NBSS\_Zmtn) showed a general decline with size and a shift in the maximum values, with the maximum of NBSS\_Zuwp representing 50% of the median values of the Multinet. Above 1.5 mm, NBSS\_Zuwp were generally higher than NBSS\_Zmtn, although size spectra were more variable among collected samples (Supplementary Fig. 1). These differences in the number of organisms detected by the two approaches result in a large offset of total C biomass. The total carbon content (see Table I for conversion factors), derived from image biovolume estimates and group-specific size-to-biomass conversion factors (Supplementary Figs 3 and 4), showed that the contribution of more delicate forms such as rhizarians, gelatinous carnivores and filter feeders to the total biomass is important compared to other living with solid forms such as crustaceans, despite the lower C content of these delicate forms (Supplementary Fig. 4). In tropical and temperate latitudinal bands, the non-crustaceans groups contributed >50% to the total plankton biomass in the epipelagic zone and ~40% in the mesopelagic zone. The rhizarians inhabiting the epipelagic layers were dominated by collodarians in the tropics and by the phaeodarians in temperate regions. Crustacean biomass was always higher than other zooplankton biomass in polar waters



**Fig. 3.** NBSS in  $\log_{10}$  scale of all zooplankton (noted Zoo) detected by the UVP5, nets and the reconstructed NBSS (maximum values) in three depth layers (0–200, 200–500 and 500–1000 m) and three latitudinal bands ( $0\text{--}30^\circ$ ,  $30\text{--}60^\circ$ ,  $>60^\circ$ ). The shaded area corresponds to the 25 and 75 quartiles around the median of all NBSS observed at the 57 stations shown in Fig. 1. The first dashed line from left corresponds to the 1 mm, while the second and third dashed lines delimit the size range used to extract and compare the NBSS slopes.

where both UVP5 and Multinet presented similar patterns. In this region, some phaeodarians were found in deeper UVP5 casts, while they were absent from Multinet samples. Gelatinous carnivorous biomass were well observed with both approaches similarly as crustaceans (Supplementary Figs 3 and 4).

### Zooplankton NBSS in three depth layers and latitudinal bands

After summing all taxon-specific size spectra to obtain NBSS<sub>Zuvp</sub> and NBSS<sub>Zmnt</sub>, we found substantial differences between zooplankton sizes distributions, notably at size larger than 1 mm in ESD mainly in the tropical latitudinal band (Supplementary Fig. 5). Above this size, NBSS<sub>Zuvp</sub> estimates generally presented higher normalized biovolume than NBSS<sub>Zmnt</sub> at multiple depths and latitudes from tropical to temperate zones. NBSS<sub>Zmnt</sub> also declined more sharply with size, indicative of steeper NBSS slopes, compared to the NBSS<sub>Zuvp</sub> (Fig. 3). In contrast, the two NBSS estimates strongly overlapped at the surface and in the upper mesopelagic zone of the polar regions. For all latitudinal bands, integrated NBSS values, used as a proxy for total zooplankton abundances, showed a decline in concentration with depth, with values in the 0–200 m depth (epipelagic) layer always greater than those in the mesopelagic layer (200–1000 m).

### Relative contribution of different taxa to zooplankton reconstructed NBSS

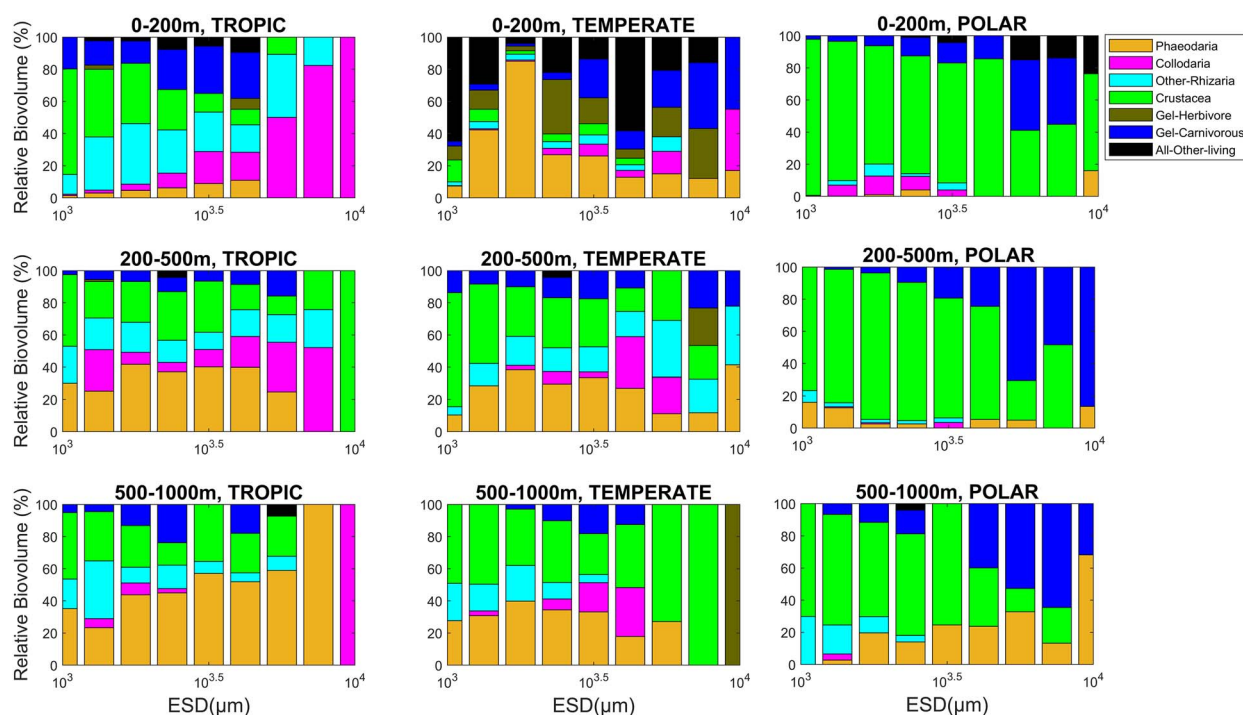
The relative contribution of the different zooplankton categories (Fig. 4) to the reconstructed NBSS showed that the main contributors to the total biovolume were crustaceans and

rhizarians (in most size fractions) and gelatinous carnivores in the largest size class. However, there was a large variability depending on the latitudinal bands and depth layers. The contribution of rhizarians to the total zooplankton biovolume in all size classes decreased from low latitudes to high latitudes in the epipelagic to mesopelagic layers. Inter-tropical samples showed that in the epipelagic layer, colpodarians dominated in the larger size fraction while in the mesopelagic layer, phaeodarians dominated in the small size fraction. In temperate samples, phaeodarians and gelatinous (carnivorous and filter feeders) dominated the biovolume at the surface while copepods and phaeodarians were dominant in the mesopelagic. In the polar regions, crustaceans largely dominated biomass and biovolume in almost all size classes except in large size classes of the lower mesopelagic layer, where carnivorous gelatinous and phaeodarians were more abundant (Supplementary Fig. 4).

### Comparison of zooplankton NBSS slopes and total biomass by different methods

The reconstruction of zooplankton NBSS was generally closer to UVP5 estimates than Multinet estimates (Fig. 3). As expected, the reconstructed NBSS closely aligned to the upper envelope of the measured NBSS and overall followed the UVP5-derived estimates more closely than the Multinet. The reconstructed total zooplankton concentration maximum also declined with depth from top layer to the bottom layer, with the epipelagic layer being on average 3 times higher than the upper mesopelagic layer and 12 times higher than the lower mesopelagic layer.

The NBSS slopes, and their variance around the median, changed with depth (Fig. 5), with flatter, less variable slopes in



**Fig. 4.** Relative contributions of different zooplankton taxa to the reconstructed NBSS (for plankton size from 1 to 8 mm) in three depth layers (0–200, 200–500 and 500–1000 m) and three latitudinal bands (0–30°, 30–60°, >60°). The top panel indicates the surface, the middle panel indicates the upper mesopelagic layer and the bottom panel for the lower mesopelagic layer. The colors represent different groups of zooplankton, and Gel- means Gelatinous.

the mesopelagic zone and steeper slopes in the epipelagic layer. The reconstructed NBSS slope appeared closer, albeit steeper, to that measured by the UVP5 and was systematically flatter than that of Multinet ( $P$ -value > 0.05). No significant differences were found between slopes from UVP5 and the reconstructed NBSS in the tropical and temperate epipelagic layers ( $P$ -value > 0.05). Differences were not significant (Supplementary Fig. 6) in the polar epipelagic layer for the three (UVP5, net, reconstructed) methods ( $P$ -values > 0.05). The linear regression between the reconstructed and the UVP5 biomass estimates (Table II) for the three latitudinal bands and the three depths layers showed that they were strongly dependent, as all  $P$ -values are significant and  $R^2$  is higher than 0.8, except in the polar epipelagic layer where it was 0.63. Similar linear regression for NBSS slopes (Table III) showed that all  $P$ -values are significant, with  $R^2$  higher than 0.7. In contrast, the correlations between Multinet data and reconstructed values were weaker, as indicated by lower  $R^2$ , and most of the linear regressions in tropic and temperate were not significant (Tables IV and V).

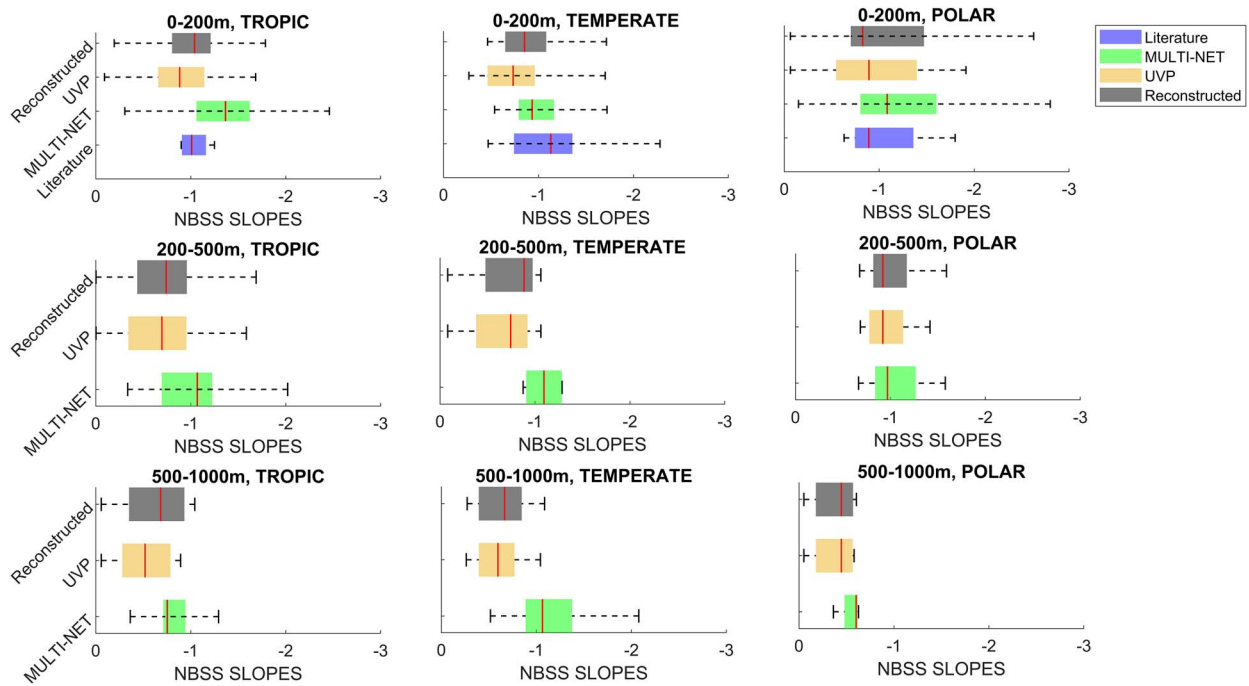
Our results showed that the reconstructed NBSS slopes were significantly flatter than the Multinet ( $\partial = -20\%$ , correlation coefficient:  $0.36 \pm 0.14$ ,  $P$ -value =  $3.75 \times 10^{-07}$ ) and steeper than the ones of UVP5 ( $\partial = +7.6\%$ , correlation coefficient:  $0.93 \pm 0.02$ ,  $P$ -value =  $5.56 \times 10^{-74}$ ).

As spectral intercepts decreased with depth, the total reconstructed zooplankton biomass of organisms larger than 1 mm presented a general decrease with depth apart from the polar region where the biomass maximum was found in the upper mesopelagic (Fig. 6). Total zooplankton biomass calculated from

the reconstructed NBSS showed a decrease from the poles to the tropics. The reconstructed biomass was systematically higher than that of the Multinet, with the largest differences observed in the tropical and temperate surface layers. In general, the biomass of the reconstructed NBSS is closer to that of UVP5 in tropics and temperate oceans and almost similar to that of multinet in polar ocean.

In the tropics, the absolute gain ( $\Delta Y$ ) in biomass (Supplementary Table II) when comparing the reconstructed and the Multinet biomass decreased with depth:  $+1.66 \text{ mgC m}^{-3}$  ( $\partial = 136\%$ ) in the surface,  $+0.81 \text{ mgC m}^{-3}$  ( $\partial = 615\%$ ) in the upper mesopelagic and  $+0.27 \text{ mgC m}^{-3}$  ( $\partial = 900\%$ ) in the lower mesopelagic. In temperate ecosystems, the absolute gains in biomass were significantly higher, with  $+3.4 \text{ mgC m}^{-3}$  ( $\partial = 309\%$ ) in the surface,  $+1.23 \text{ mgC m}^{-3}$  ( $\partial = 440.1\%$ ) in the upper mesopelagic and  $+0.77 \text{ mgC m}^{-3}$  ( $\partial = 440.5\%$ ) in the lower mesopelagic. In polar ecosystems, the gains ( $\Delta Y$ ) were much lower, with  $+0.24 \text{ mgC m}^{-3}$  ( $\partial = 4.25\%$ ) in the surface,  $+2.71 \text{ mgC m}^{-3}$  ( $\partial = 26\%$ ) in the upper mesopelagic and  $+0.68 \text{ mgC m}^{-3}$  ( $\partial = 31.66\%$ ) in the lower mesopelagic.

The same trends were observed when comparing the reconstructed biomass to that of the UVP5, although gains were generally more marginal. In the tropics, the average absolute gain in biomass ranged from  $+0.04 \text{ mgC m}^{-3}$  ( $\partial = 14.2\%$ ) and  $+0.08 \text{ mgC m}^{-3}$  ( $\partial = 6.56\%$ ) in the lower and upper mesopelagic, to  $+0.67 \text{ mgC m}^{-3}$  ( $\partial = 30.44\%$ ) in the surface. In temperate ecosystems, the gain in biomass was on average  $+0.74 \text{ mgC m}^{-3}$  ( $\partial = 19.59\%$ ),  $+0.74 \text{ mgC m}^{-3}$  ( $\partial = 97\%$ ) and  $+0.024 \text{ mgC m}^{-3}$  ( $\partial = 2.71\%$ ), respectively in the epipelagic, upper and



**Fig. 5.** Comparison of mesozooplankton NBSS slopes from the three methods (UVP5, net, reconstructed) at different locations in three depth layers (0–200, 200–500 and 500–1000 m) and three latitudinal bands (0–30°, 30–60°, >60°) for plankton ESD from 1 to 8 mm. Our study data are from Multinet and UVP5. A compilation of literature slopes from the previous studies (Dai *et al.*, 2016, 2017) from the epipelagic layer was used to compare our results. The boxes represent the 25 and 75 quartiles around the median value. The dashed line show the limit for the outliers.

**Table II:** Linear regressions between the reconstructed biomass and the UVP5 biomass

Latitude & depth (biomass, mgC m <sup>-3</sup> )	Equation Y = Ax + B	P-value	R2
Tropic 0–200 m	Y = 1.01X <sub>uvp</sub> + 1.44	6.25 × 10 <sup>-53</sup>	0.96 ***
Tropic 200–500 m	Y = 1.04X <sub>uvp</sub> + 0.06	7.99 × 10 <sup>-62</sup>	0.98 ***
Tropic > 500 m	Y = 0.995X <sub>uvp</sub> + 0.02	6.59 × 10 <sup>-41</sup>	0.99 ***
Temperate 0–200 m	Y = 1.285X <sub>uvp</sub> - 0.21	2.63 × 10 <sup>-07</sup>	0.84 ***
Temperate 200–500 m	Y = 1.13X <sub>uvp</sub> + 0.096	5.39 × 10 <sup>-09</sup>	0.95 ***
Temperate > 500 m	Y = 0.998X <sub>uvp</sub> + 0.03	4.92 × 10 <sup>-12</sup>	0.99 ***
Polar 0–200 m	Y = 1.13X <sub>uvp</sub> + 9.11	1.12 × 10 <sup>-06</sup>	0.63 ***
Polar 200–500 m	Y = 0.95X <sub>uvp</sub> + 4.95	1.89 × 10 <sup>-05</sup>	0.85 ***
Polar > 500 m	Y = 1.10X <sub>uvp</sub> + 0.19	0.027	0.84 *

The symbols are: \* if P-value <0.05, \*\* if P-value <0.01, \*\*\* if P-value <0.001 and ns for non-significant or P-value >0.05

**Table III:** Linear regressions between the reconstructed slopes and the UVP5 slopes

Latitude & depth (slopes)	Equation Y = Ax + B	P-value	R2
Tropic 0–200 m	Y = 0.86X <sub>uvp</sub> - 0.25	2.82 × 10 <sup>-20</sup>	0.80 ***
Tropic 200–500 m	Y = 1.00X <sub>uvp</sub> - 0.05	1.7 × 10 <sup>-24</sup>	0.92 ***
Tropic > 500 m	Y = 1.02X <sub>uvp</sub> - 0.09	4.64 × 10 <sup>-04</sup>	0.76 ***
Temperate 0–200 m	Y = 0.78X <sub>uvp</sub> - 0.29	2.32 × 10 <sup>-06</sup>	0.85 ***
Temperate 200–500 m	Y = 0.98X <sub>uvp</sub> - 0.07	2.50 × 10 <sup>-06</sup>	0.92 ***
Temperate > 500 m	Y = 1.06X <sub>uvp</sub> - 0.01	8.85 × 10 <sup>-04</sup>	0.95 ***
Polar 0–200 m	Y = 1.35X <sub>uvp</sub> + 0.1	3.13 × 10 <sup>-06</sup>	0.73 ***
Polar 200–500 m	Y = 0.96X <sub>uvp</sub> - 0.08	8.79 × 10 <sup>-04</sup>	0.73 ***
Polar > 500 m	Y = 1.02X <sub>uvp</sub> + 0.001	4.36 × 10 <sup>-04</sup>	0.99 ***

The symbols are: \* if P-value <0.05, \*\* if P-value <0.01, \*\*\* if P-value <0.001 and ns for non-significant or P-value >0.05



**Table IV:** Linear regressions between the reconstructed biomass and the Multinet biomass

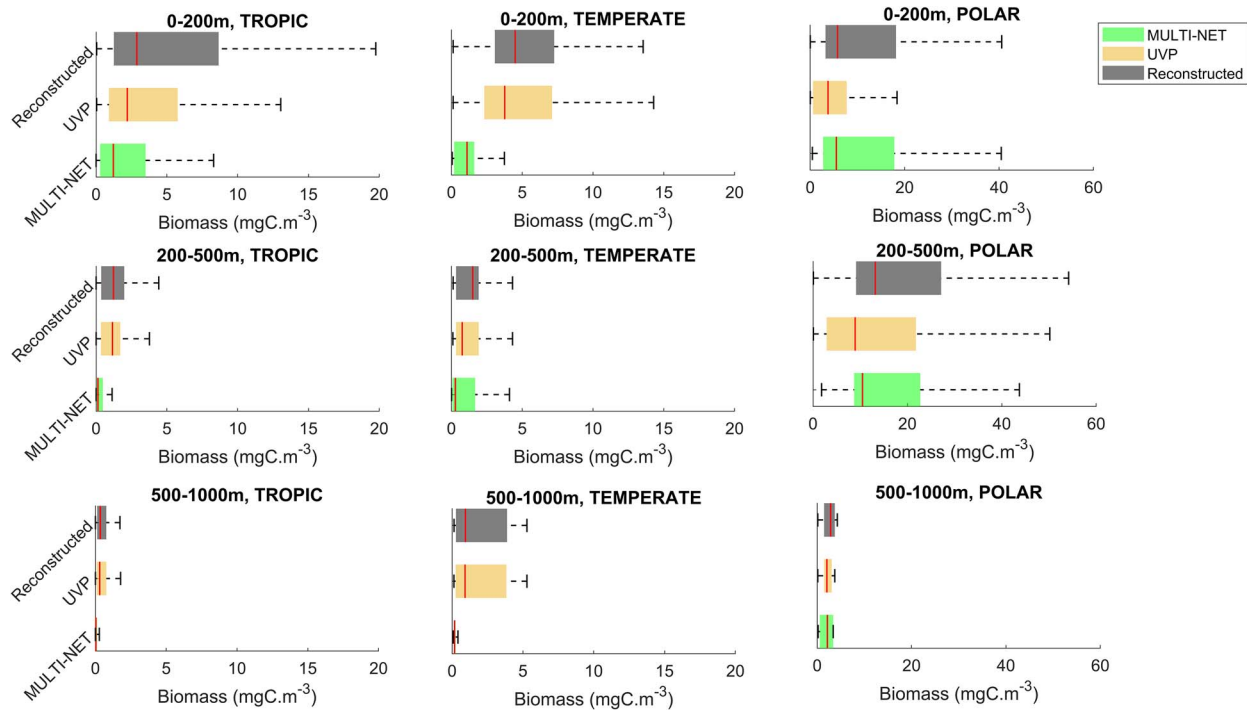
Latitude & depth (biomass, mgC m <sup>-3</sup> )	Equation Y = Ax + B	P-value	R2
Tropic 0–200 m	Y = 1.34X <sub>net</sub> + 2.48	1.14 × 10 <sup>-13</sup>	0.57 ***
Tropic 200–500 m	Y = 1.55X <sub>net</sub> + 1.09	3.29 × 10 <sup>-05</sup>	0.23 ***
Tropic > 500 m	Y = 2.36X <sub>net</sub> + 0.76	0.51	0.0197 ns
Temperate 0–200 m	Y = 1.14X <sub>net</sub> + 3.62	1.2 × 10 <sup>-04</sup>	0.64 ***
Temperate 200–500 m	Y = 1.27X <sub>net</sub> + 0.61	1.84 × 10 <sup>-06</sup>	0.88 ***
Temperate > 500 m	Y = 2.81X <sub>net</sub> + 1.25	0.48	0.085 ns
Polar 0–200 m	Y = 1.11X <sub>net</sub> + 2.13	6.79 × 10 <sup>-11</sup>	0.86 ***
Polar 200–500 m	Y = 1.08X <sub>net</sub> + 2.72	5.13 × 10 <sup>-06</sup>	0.91 ***
Polar > 500 m	Y = 0.57X <sub>net</sub> + 2.02	0.067	0.87 ns

The symbols are: \* if P-value < 0.05, \*\* if P-value < 0.01, \*\*\* if P-value < 0.001 and ns for non-significant or P-value > 0.05

**Table V:** Linear regressions between the reconstructed slopes and Multinet slopes

Latitude & depth (slopes)	Equation Y = Ax + B	P-value	R2
Tropic 0–200 m	Y = 0.25X <sub>net</sub> - 0.73	2.71 × 10 <sup>-03</sup>	0.22 ***
Tropic 200–500 m	Y = 0.10X <sub>net</sub> - 0.66	0.388	0.021 ns
Tropic > 500 m	Y = -0.31X <sub>net</sub> - 0.90	0.398	0.15 ns
Temperate 0–200 m	Y = 0.44X <sub>net</sub> - 0.40	0.138	0.23 ns
Temperate 200–500 m	Y = 0.166X <sub>net</sub> - 0.75	0.567	0.07 ns
Temperate > 500 m	Y = 0.11X <sub>net</sub> - 0.52	0.71	0.04 ns
Polar 0–200 m	Y = 0.72X <sub>net</sub> - 0.13	6.11 × 10 <sup>-08</sup>	0.87 ***
Polar 200–500 m	Y = 0.70X <sub>net</sub> - 0.28	2.72 × 10 <sup>-03</sup>	0.65 ***
Polar > 500 m	Y = 1.67X <sub>net</sub> + 0.56	0.218	0.61 ns

The symbols are: \* if P-value < 0.05, \*\* if P-value < 0.01, \*\*\* if P-value < 0.001 and ns for non-significant or P-value > 0.05



**Fig. 6.** Comparison of mesozooplankton biomass from the three methods (UVP5, net, reconstructed) at different locations in three depth layers (0–200, 200–500 and 500–1000 m), and three latitudinal bands (0–30°, 30–60°, >60°) for plankton ESD from 1 to 8 mm. Our study data are from Multinet and UVP5. The boxes represent the 25 and 75 quartiles around the median value. The dashed line shows the limit for the outliers.

lower mesopelagic layers. In the same depth layers, polar ecosystems biomass gain was  $+2.0 \text{ mgC m}^{-3}$  ( $\partial = 53\%$ ),  $+4.27 \text{ mgC m}^{-3}$  ( $\partial = 48\%$ ) and  $+0.78 \text{ mgC m}^{-3}$  ( $\partial = 38\%$ ) from surface to mesopelagic layers.

## DISCUSSION

Here, we provide a comprehensive dataset of zooplankton NBSS based on individual measurements of body size and document the shape of the size spectrum obtained from two imaging approaches on a global scale. Previous zooplankton studies have mostly reported NBSS estimates based on nets data or total biomass from UVP5 data (Forest *et al.*, 2012; Biard *et al.*, 2016; Drago *et al.*, 2022). Here, we report new, holistic, zooplankton size distribution estimates across the global ocean, using the combination of both net and UVP approaches. In the following sections, we compare our UVP5 and net datasets to other studies so far restricted to specific oceanic regions; we discuss discrepancies between each approach and finally highlight the novel understanding of the reconstructed NBSS.

### Comparison of zooplankton size structure and biomass with existing case studies

We find that zooplankton communities collected with nets exhibit maximum NBSS and biomass values toward the poles, a pattern that is largely driven by crustaceans. This pattern is induced by the higher contributions of the large-size grazing Calanidae in the polar waters compared to the dominance of smaller omnivorous–carnivorous Cyclopoida and Poecilostomatoida (i.e. Oithonidae, Oncaeiidae and Corycaeiidae) in tropical regions (Brandão *et al.*, 2021; Soviadan *et al.*, 2022). It is also well known that zooplankton size, along with abundance and biomass, decreases from high temperature and increases at higher relative contribution of small phytoplankton. While it increases with concentrations of oxygen, macronutrients, total phytoplankton biomass and the relative contribution of large phytoplankton (Brun *et al.*, 2016; Brandão *et al.*, 2021; Soviadan *et al.*, 2022). This latitudinal trend is consistent with other observations of high copepod abundance or biomass in the polar ecosystems (Hirche and Mumm, 1992; Balazy *et al.*, 2018; Pinkerton *et al.*, 2020; Drago *et al.*, 2022). Our results also agree with recent *in situ* imaging data compilation and model output that found that polar waters are dominated by Copepoda, whereas in the intertropical waters, mixotrophic rhizarians represent a more substantial part of the biomass (Biard *et al.*, 2016; Drago *et al.*, 2022). The median mesozooplankton biomass found in the present study, which varied from 1.3–2.9  $\text{mgC m}^{-3}$  in the epipelagic layer (Supplementary Fig. 6), is also within the range of biomass reported in the COPEPOD global database (Moriarty and O'Brien, 2013) with values of 0.98–3.6  $\text{mgC m}^{-3}$ .

Despite the significant impact of the previously undersampled rhizarians on NBSS slopes derived from the UVP5 (see next section), especially in tropical and temperate regions, we focus our comparison on global datasets of zooplankton NBSS slopes obtained with nets, as they are the only values reported in the literature to our knowledge (Dai *et al.*, 2016, 2017).

The NBSS slopes calculated from the Multinet collection (NBSS\_Zmtn) were compared with a global compilation gleaned from the literature (Supplementary Table III). The comparison showed that the reported values are well within the range of observed values and that they show a contrasting spatial distribution around the globe, consistent with the variability observed between low-productivity and high-productivity systems. In our study, the median slopes of the normalized biovolume size spectra were generally flatter than  $-1$  (ranging from  $-0.57$  to  $-0.94$ ), which indicates that zooplankton communities in the study area were characterized by high energy transfer efficiency. The NBSS median slopes from this study were more moderate than those in the North Pacific Ocean, Northwest Pacific Ocean, Northwest Atlantic Ocean, California Current, California Bight and Western Antarctic Peninsula (see Table 3 in Dai *et al.*, 2016). The median NBSS slopes computed from UVP5 were systematically flatter than the net-collected zooplankton slopes, and also those from the literature, presumably because of the better efficiency of UVP5 in capturing larger, fragile organisms.

In our study, steeper slopes were observed in shallower strata compared to the mesopelagic. Smaller-sized organisms may prevail in the upper water layer (Ohman and Romagnan, 2016), as they feed on smaller prey such as the phytoplankton and other microzooplankton prey. Being small may be an advantage for escaping predators, but this surface layer is also an important reproductive layer where all types of larvae prevail. Higher average size or flatter slopes of organisms in the mesopelagic reflect the relative importance of larger-sized individuals in the deep ocean (Ohman and Romagnan, 2016). Deep ocean environments may favor larger individuals through multiple mechanisms favoring their survival. For instance, environmental factors such as lower temperature, less dissolved oxygen and increased hydrostatic pressure (Childress, 1995) could have decreased the selective pressure for high activity (“predation-mediated selection” hypothesis). Larger individuals perform better in deep environments because they can accumulate more energy to survive (Hopcroft *et al.*, 2001). However, an increased trophic level can also lead to corresponding increases in body size (Romero-Romero *et al.*, 2016). The biomass of phytoplankton declines with depth (Yamaguchi *et al.*, 2002), so the predator–prey relationship typically shifts from more herbivorous to a more omnivorous or carnivorous ratio (Vinogradov and Tseitlin, 1983). Furthermore, from an individual perspective, deeper-living pelagic species use more energy to achieve larger sizes, although they have lower energy concentrations and metabolic rates (Childress *et al.*, 1990).

### Discrepancy in zooplankton NBSS assessed *in situ* and *ex situ* with potential corrections

Our results demonstrate that assessing zooplankton NBSS and total biomass from samples collected by plankton nets or detected by *in situ* cameras may differ significantly. Many studies have demonstrated that plankton assessment is subjective to the protocol used for collection and analysis (Benfield *et al.*, 1998; Harris *et al.*, 2000; Wiebe and Benfield, 2003; Remsen *et al.*, 2004; Forest *et al.*, 2012). However, in the specific case

of the Arctic, good agreement was found between net-collected zooplankton and organisms detected *in situ* (Forest *et al.*, 2012).

It is well known that nets may discard small organisms as a function of mesh size and destroy fragile organisms (Remsen *et al.*, 2004). *In situ* imaging may be more appropriate for such fragile plankton (Remsen *et al.*, 2004; Biard *et al.*, 2016) notably in the upper ocean of intertropical regions where large rhizarians (mostly collodarians) predominate. However, a major drawback of *in situ* cameras is the smaller-imaged volume, leading to inaccurate analysis of community composition, especially large rare organisms, from single casts (Stemmann *et al.*, 2008; Picheral *et al.*, 2010; Lombard *et al.*, 2019). Consistent patterns can, however, emerge when aggregating multiple UVP5 profiles for each station and/or aggregating results from similar habitats according to latitude and depth, similarly to our study. In addition, the taxonomic resolution achieved by *in situ* images is much lower than the taxonomic resolution obtained from net samples scanned with a ZooScan. Due to this methodological bias and to be as accurate as possible, this study focused on organisms larger than ESD > 1 mm. In the size range ESD < 1 mm, many of the particles were identified as marine snow, larvacean houses, diatom rafts, or fecal pellet strings, which we discarded in our analysis as they did not constitute living zooplankton. However, we note that the majority of our unclassified images were of particles smaller than 1 mm ESD, which lacked any resolvable characteristics to support their identification. It is possible that the bias in NBSS due to rhizarians observed in the ESD > 1 mm size range could be important in the 200  $\mu\text{m}$ –1 mm size range. Future studies should address this issue over a greater size range.

Crustaceans and carnivorous gelatinous were the best represented groups in both UVP and Multinet NBSS across all samples. This suggests that UVP5 sampled well crustaceans especially in polar regions where their size is bigger, even though the volume imaged was more limited. Forest *et al.* (2012) and Barth and Stone (2022) observed that the UVP5 did not sample copepods accurately below 1 mm ESD. Using copepods as benchmark, since they were abundant and not damaged by the net collection, we showed that for organisms larger than 1 mm in ESD, both biomass estimates were generally in agreement in polar regions dominated by crustaceans. Hence in this region, the difference in modal sizes of the zooplankton NBSS was mainly due to difference in the image resolutions, rather than by a difference in community composition.

To correct the biomass and slopes measured from each instrument, depending on the latitudinal zone and depth of samples, we propose the relative gain in biomass and change in slopes (noted  $\partial$ ) or the linear regression between the reconstructed values and the measured values when the  $R^2$  is positive and the  $P$ -value < 0.05. The linear function correction worked better for UVP5 than the Multinet.

### Novel understanding of pelagic ecology gained by combining *in situ* and net collected data

Our analysis on a global scale mostly in the open ocean allows us to draw general conclusions on the relationship between NBSS estimated from *in situ* devices and those estimated from net samples. Compared to previous works based on nets samples, the reconstructed NBSS are flatter for tropical and temperate waters

and relatively similar in polar waters. The UVP5 slopes are flatter than slopes obtained with other methods (net and reconstructed NBSS). The slopes of the reconstructed NBSS are steeper than the UVP5 and flatter than the Multinet modifying the transfer efficiency estimates from the past studies and the estimation of carbon flow in the food web and in vertical pump. The large variability among slopes of the same latitudinal bands, especially in the epipelagic and upper mesopelagic layers, can be due to the biogeographical conditions and temporal factors (coastal/off-shore samples, eutrophic/oligotrophic zones and date of cruises) affecting our sampling. In general, the reconstructed slopes were higher than  $-1$ , meaning that the transfer efficiency of carbon was good or stable. The reconstructed slopes reveal a stable ecosystem in the tropic regions and good transfer of biomass in temperate and polar ecosystems, particularly in the surface layer.

The main reason for the modification of the NBSS is due to the fragile rhizarians that were not accounted for when using net data. The average size of the rhizarians found in the UVP5 samples was higher than crustaceans. This suggests that much of plankton biovolume is missed in the net catches mostly taken in inter-tropical regions. In upper mesopelagic samples of intertropical regions, rhizarians' contribution to the total biomass is similar to the contribution of crustaceans; however, their contribution decreased with depth. We note that we observed a strong variability of these estimates, depending on the type of the ecosystem and the balance between the fraction of crustaceans (mainly copepods) and rhizarians. It is noticeable that the contribution of large phaeodarians is more important in the mesopelagic layer than in the epipelagic layer where collodarians are important. The rhizarians detected by the UVP5 and the crustaceans well sampled by the net bring together new pieces to the reconstruction of the NBSS and slopes that may change our assessment of the flow of energy in trophic web when using only net data. The fact that rhizarians are missing in the net leads to underestimation of the energy flow in the food web structure and pose the question of their inclusion in future biogeochemical modeling as their impact on the efficiency of carbon pump could be important.

## CONCLUSION

We report here, for the first time at global scale, the zooplankton biovolume and carbon biomass estimated in the upper kilometer by the combination of two mature, but biased, sampling methods. *In situ* imaging with UVP5 allows to detect all organisms including fragile ones, albeit in a small sampled volume (several hundreds of liters for each profile), while Multinet combined with ZooScan image analysis samples a large volume (several tens of inverse cubic meters for each sample), but damages fragile organisms. The optimal values measured by both methods are used to reconstruct the zooplankton biovolume and biomass distributions.

Our results showed that the reconstructed NBSS slopes were indeed the golden mean, as they were flatter than the ones obtained from Multinet ( $\partial = -20\%$ ) and steeper than those obtained from the UVP5 ( $\partial = +7.6\%$ ). This suggests that Multinets significantly undersample large and fragile organisms because of destruction or avoidance whereas UVP5 is lacking

good resolution for the smaller organisms. Large differences between methods were systematically observed in ecosystems dominated by rhizarians, namely, the tropical and temperate regions including surface and mesopelagic layers. Thus, the overall biomass gain in surface layer when we compared the reconstructed biomass to the bulk estimates from Multinet was  $+0.24 \text{ mgC m}^{-3}$  (+4.25%) and is rather high when we compared the reconstructed biomass to the UVP5 biomass ( $+2.0 \text{ mgC m}^{-3}$  or +53%) in the polar region. In contrast, the biomass gain from UVP5 in tropical and temperate ecosystems was, respectively,  $+0.67 \text{ mgC m}^{-3}$  (+30.44%) and  $+0.74 \text{ mgC m}^{-3}$  (19.59%) and the biomass gain from Multinet was, respectively,  $+1.66 \text{ mgC m}^{-3}$  (+136%) and  $+3.4 \text{ mgC m}^{-3}$  (+309%) in tropical and temperate ecosystems. In the mesopelagic layer, there are less differences with reconstructed biomass when we used UVP5 in comparison to Multinet. These differences suggest that rhizarians, when abundant, have a profound impact on the slope of the NBSS. These biases limit our ability to use only NBSS calculated from net collected samples as an indicator of the trophic flow of energy while their advantage is provided by their higher taxonomic resolution. Lower observed volume and resolution prevents the use of the UVP5 alone to study mesozooplankton biodiversity. Therefore, with current technologies, we suggest to combine both methods because the complementarity of *in situ* imaging technologies together with nets sampling provides a more complete dataset to study ecosystems functioning, using NBSS as a key planktonic variable.

#### ACKNOWLEDGEMENTS

Tara Oceans (which includes both the Tara Oceans and Tara Oceans Polar Circle expeditions) would not exist without the leadership of the Tara Ocean Foundation and the continuous support of 23 institutes (<https://oceans.taraexpeditions.org/>). The global sampling effort was enabled by countless scientists and crew who sampled aboard the Tara from 2009 to 2013, and we thank MERCATOR-CORIOLIS and ACRI-ST for providing daily satellite data during the expeditions. We are also grateful to the countries who graciously granted sampling permission. We thank Agnès b. and Etienne Bourgois, the Prince Albert II de Monaco Foundation, the Veolia Foundation, Region Bretagne, Lorient Agglomeration, Serge Ferrari, Worldcourier and KAUST for support and commitment. We also thank “Make Our Planet Great Again Team” for the postdoctoral fellow support.

#### FUNDING

Centre National de Recherche Scientifique in particular Groupe de Recherche [GDR3280], the Research Federation for the Study of Global Ocean Systems Ecology and Evolution [FR2022/Tara-Oceans GOSEE], the European Molecular Biology Laboratory, the French Ministry of Research and the French Government “Investissements d’Avenir” programs OCEANOMICS [ANR-11-BTBR-0008] and the EMBRC-France [ANR-10-INBS-02]. D.S., L.D., R.K. and L.S. received support by the European Union project TRIATLAS (European Union Horizon 2020 program, grant agreement 817578) and the Sorbonne Université through the Ecole doctorale 129. D.S. was supported by the Fond Français pour l’Environnement

Mondial and the Make Our Planet Great Again fellowships. R.K. acknowledges support via a Make Our Planet Great Again grant from the French National Research Agency (ANR) within the Programme d’Investissements d’Avenir #ANR-19-MPGA-0012 and funding from the Heisenberg Programme of the German Science Foundation #KI 1387/5-1. L.S. was supported for the initial phase by the Chair VISION from CNRS/Sorbonne University. Grants for the collection and processing of the Tara Oceans data set were provided by NASA Ocean Biology and Biogeochemistry Program to the University of Maine; the Canada Excellence research chair on remote sensing of Canada’s new Arctic frontier; and the Canada Foundation for Innovation under [grants numbers NNX11AQ14G, NNX09AU43G, NNX13AE58G and NNX15AC08G].

#### SUPPLEMENTARY DATA

Supplementary data can be found at *Journal of Plankton Research* online.

#### DATA AVAILABILITY

Multinet data and UVP5 are published in PANGAEA. Additional supplementary material was submitted as online Supplementary Material.

#### REFERENCES

- Atkinson, A., Rossberg, A. G., Gaedke, U., Sprules, G., Heneghan, R. F., Batziakas, S., Grigoratou, M., Fileman, E. *et al.* (2024) Steeper size spectra with decreasing phytoplankton biomass indicate strong trophic amplification and future fish declines. *Nat. Commun.*, **15**, 381. <https://doi.org/10.1038/s41467-023-44406-5>.
- Balazy, K., Trudnowska, E., Wichorowski, M. and Błachowiak-Samołyk, K. (2018) Large versus small zooplankton in relation to temperature in the Arctic shelf region. *Polar Res.*, **37**, 1427409. <https://doi.org/10.1080/17518369.2018.1427409>.
- Barth, A. and Stone, J. (2022) Comparison of an *In situ* imaging device and net-based method to study Mesozooplankton communities in an oligotrophic system. *Front. Mar. Sci.*, **9**, 1–14, 898057. <https://doi.org/10.3389/fmars.2022.898057>.
- Bathmann, U., Bundy, M. H., Clarke, M. E., Cowles, T. J., Daly, K., Dam, H. G., Deksheniaks, M. M., Donaghay, P. L. *et al.* (2001) Future marine zooplankton research - a perspective. *Mar. Ecol. Prog. Ser.*, **222**, 297–308. <https://doi.org/10.3354/meps222297>.
- Benfield, M. C., Grosjean, P., Culverhouse, P. F., Irigoien, X., Sieracki, M. E., Lopez-Urrutia, A., Dam, H. G., Hu, Q. *et al.* (2007) RAPID: research on automated plankton identification. *Oceanography*, **20**, 172–187. <https://doi.org/10.5670/oceanog.2007.63>.
- Benfield, M. C., Wiebe, P. H., Stanton, T. K., Davis, C. S., Gallager, S. M. and Greene, C. H. (1998) Estimating the spatial distribution of zooplankton biomass by combining video plankton recorder and single-frequency acoustic data. *Deep-Sea Res. II Top. Stud. Oceanogr.*, **45**, 1175–1199. [https://doi.org/10.1016/S0967-0645\(98\)00026-5](https://doi.org/10.1016/S0967-0645(98)00026-5).
- Biard, T., Stemann, L., Picheral, M., Mayot, N., Vandromme, P., Hauss, H., Gorsky, G., Guidi, L. *et al.* (2016) *In situ* imaging reveals the biomass of giant protists in the global ocean. *Nature*, **532**, 504–507. <https://doi.org/10.1038/nature17652>.
- Boyd, P. W., Claustre, H., Levy, M., Siegel, D. A. and Weber, T. (2019) Multi-faceted particle pumps drive carbon sequestration in the ocean. *Nature*, **568**, 327–335. <https://doi.org/10.1038/s41586-019-1098-2>.
- Brandão, M. C., Benedetti, F., Martini, S., Soviadan, Y. D., Irissou, J.-O., Romagnan, J.-B., Elineau, A., Desnos, C. *et al.* (2021) Macroscale

- patterns of oceanic zooplankton composition and size structure. *Sci. Rep.*, **11**, 15714. <https://doi.org/10.1038/s41598-021-94615-5>.
- Brun, P., Payne, M. R. and Kjørboe, T. (2016) Trait biogeography of marine copepods - an analysis across scales. *Ecol. Lett.*, **19**, 1403–1413. <https://doi.org/10.1111/ele.12688>.
- Cavan, E. L., Henson, S. A., Belcher, A. and Sanders, R. (2017) Role of zooplankton in determining the efficiency of the biological carbon pump. *Biogeosciences*, **14**, 177–186. <https://doi.org/10.5194/bg-14-177-2017>.
- Childress, J. J. (1995) Are there physiological and biochemical adaptations of metabolism in deep-sea animals? *Trends Ecol. Evol.*, **10**, 30–36. [https://doi.org/10.1016/S0169-5347\(00\)88957-0](https://doi.org/10.1016/S0169-5347(00)88957-0).
- Childress, J. J., Cowles, D. L., Favuzzi, J. A. and Mickel, T. J. (1990) Metabolic rates of benthic deep-sea decapod crustaceans decline with increasing depth primarily due to the decline in temperature. *Deep Sea Res. A Oceanogr. Res. Pap.*, **37**, 929–949. [https://doi.org/10.1016/0198-0149\(90\)90104-4](https://doi.org/10.1016/0198-0149(90)90104-4).
- Christiansen, S., Hoving, H.-J., Schuette, F., Hauss, H., Karstensen, J., Koertzienger, A., Schroeder, S.-M., Stemmann, L. et al. (2018) Particulate matter flux interception in oceanic mesoscale eddies by the polychaete *Poebobius* sp. *Limnol. Oceanogr.*, **63**, 2093–2109. <https://doi.org/10.1002/lno.10926>.
- Dai, L., Li, C., Tao, Z., Yang, G., Wang, X. and Zhu, M. (2017) Zooplankton abundance, biovolume and size spectra down to 3000m depth in the western tropical North Pacific during autumn 2014. *Deep-Sea Res. I Oceanogr. Res. Pap.*, **121**, 1–13. <https://doi.org/10.1016/j.dsr.2016.12.015>.
- Dai, L., Li, C., Yang, G. and Sun, X. (2016) Zooplankton abundance, biovolume and size spectra at western boundary currents in the subtropical North Pacific during winter 2012. *J. Mar. Syst.*, **155**, 73–83. <https://doi.org/10.1016/j.jmarsys.2015.11.004>.
- Dennett, M. R., Caron, D. A., Michaels, A. F., Gallager, S. M. and Davis, C. S. (2002) Video plankton recorder reveals high abundances of colonial Radiolaria in surface waters of the central North Pacific. *J. Plankton Res.*, **24**, 797–805. <https://doi.org/10.1093/plankt/24.8.797>.
- Drago, L., Panaïotis, T., Irisson, J.-O., Babin, M., Biard, T., Carlotti, F., Coppola, L., Guidi, L. et al. (2022) Global distribution of zooplankton biomass estimated by *in situ* imaging and machine learning. *Front. Mar. Sci.*, **9**, 1–18, 894372. <https://doi.org/10.3389/fmars.2022.894372>.
- Faure, E., Not, F., Benoiston, A.-S., Labadie, K., Bittner, L. and Ayata, S.-D. (2019) Mixotrophic protists display contrasted biogeographies in the global ocean. *ISME J.*, **13**, 1072–1083. <https://doi.org/10.1038/s41396-018-0340-5>.
- Forest, A., Stemmann, L., Picheral, M., Burdorf, L., Robert, D., Fortier, L. and Babin, M. (2012) Size distribution of particles and zooplankton across the shelf-basin system in southeast Beaufort Sea: combined results from an Underwater Vision Profiler and vertical net tows. *Biogeosciences*, **9**, 1301–1320. <https://doi.org/10.5194/bg-9-1301-2012>.
- Frangoulis, C., Psarra, S., Zervakis, V., Meador, T., Mara, P., Gogou, A., Zervoudaki, S., Giannakourou, A. et al. (2010) Connecting export fluxes to plankton food-web efficiency in the Black Sea waters inflowing into the Mediterranean Sea. *J. Plankton Res.*, **32**, 1203–1216. <https://doi.org/10.1093/plankt/fbq010>.
- Frederiksen, M., Edwards, M., Richardson, A. J., Halliday, N. C. and Wanless, S. (2006) From plankton to top predators: bottom-up control of a marine food web across four trophic levels. *J. Anim. Ecol.*, **75**, 1259–1268. <https://doi.org/10.1111/j.1365-2656.2006.01148.x>.
- Gallienne, C. P. and Robins, D. B. (2001) Is *Oithona* the most important copepod in the world's oceans? *J. Plankton Res.*, **23**, 1421–1432. <https://doi.org/10.1093/plankt/23.12.1421>.
- García-Comas, C., Chang, C.-Y., Ye, L., Sastri, A. R., Lee, Y.-C., Gong, G.-C. and Hsieh, C. (2014) Mesozooplankton size structure in response to environmental conditions in the East China Sea: how much does size spectra theory fit empirical data of a dynamic coastal area? *Prog. Oceanogr.*, **121**, 141–157. <https://doi.org/10.1016/j.poc.2013.10.010>.
- Giering, S. L. C., Culverhouse, P. F., Johns, D. G., McQuatters-Gollop, A. and Pitois, S. G. (2022) Are plankton nets a thing of the past? An assessment of *in situ* imaging of zooplankton for large-scale ecosystem assessment and policy decision-making. *Front. Mar. Sci.*, **9**, 1–13, 986206. <https://doi.org/10.3389/fmars.2022.986206>.
- Gómez-Canchong, P., Blanco, J. M. and Quiñones, R. A. (2013) On the use of biomass size spectra linear adjustments to design ecosystem indicators. *Sci. Mar.*, **77**, 257–268. <https://doi.org/10.3989/scimar.03708.22A>.
- Gorsky, G., Ohman, M. D., Picheral, M., Gasparini, S., Stemmann, L., Romagnan, J.-B., Cawood, A., Pesant, S. et al. (2010) Digital zooplankton image analysis using the ZooScan integrated system. *J. Plankton Res.*, **32**, 285–303. <https://doi.org/10.1093/plankt/fbp124>.
- Gowing, M. M. and Bentham, W. N. (1994) Feeding ecology of phaeodarian radiolarians at the VERTEX North Pacific time series site. *J. Plankton Res.*, **16**, 707–719. <https://doi.org/10.1093/plankt/16.6.707>.
- Gowing, M. M. and Wishner, K. F. (1992) Feeding ecology of benthopelagic zooplankton on an eastern tropical Pacific seamount. *Mar. Biol.*, **112**, 451–467. <https://doi.org/10.1007/BF00356291>.
- Harris, R., Wiebe, P., Lenz, J., Skjoldal, H. R. and Huntley, M. (2000) ICES Zooplankton Methodology Manual, 1–221.
- Hatton, I. A., Heneghan, R. F., Bar-On, Y. M. and Galbraith, E. D. (2021) The global ocean size spectrum from bacteria to whales. *Sci. Adv.*, **7**, eabh3732. <https://doi.org/10.1126/sciadv.abh3732>.
- Heneghan, R. F., Hatton, I. A. and Galbraith, E. D. (2019) Climate change impacts on marine ecosystems through the lens of the size spectrum. *Emerg. Top. Life Sci.*, **3**, 233–243. <https://doi.org/10.1042/ETLS20190042>.
- Hirche, H.-J. and Mumm, N. (1992) Distribution of dominant copepods in the Nansen Basin, Arctic Ocean, in summer. *Deep Sea Res. A Oceanogr. Res. Pap.*, **39**, S485–S505. [https://doi.org/10.1016/S0198-0149\(06\)80017-8](https://doi.org/10.1016/S0198-0149(06)80017-8).
- Hopcroft, R. R., Roff, J. C. and Chavez, F. P. (2001) Size paradigms in copepod communities: a re-examination. *Hydrobiologia*, **453/454**, 133–141. <https://doi.org/10.1023/A:1013167917679>.
- Irisson, J.-O., Ayata, S.-D., Lindsay, D., Karp-Boss, L. and Stemmann, L. (2022) Machine learning for the study of plankton and marine snow from images. *Annu. Rev. Mar. Sci.*, **14**, 277–301. <https://doi.org/10.1146/annurev-marine-041921-013023>.
- Karsenti, E., Acinas, S. G., Bork, P., Bowler, C., Vargas, C. D., Raes, J., Sullivan, M., Arendt, D. et al. (2011) A holistic approach to marine ecosystems biology. *PLoS Biol.*, **9**, e1001177. <https://doi.org/10.1371/journal.pbio.1001177>.
- Kiko, R., Picheral, M., Antoine, D., Babin, M., Berline, L., Biard, T., Boss, E., Brandt, P. et al. (2022) A global marine particle size distribution dataset obtained with the Underwater Vision Profiler 5. *Earth Syst. Sci. Data*, **14**, 4315–4337. <https://doi.org/10.5194/essd-14-4315-2022>.
- Ljungström, G., Claireaux, M., Fiksen, Ø. and Jørgensen, C. (2020) Body size adaptations under climate change: zooplankton community more important than temperature or food abundance in model of a zooplanktivorous fish. *Mar. Ecol. Prog. Ser.*, **636**, 1–18. <https://doi.org/10.3354/meps13241>.
- Lombard, F., Boss, E., Waite, A. M., Vogt, M., Uitz, J., Stemmann, L., Sosik, H. M., Schulz, J. et al. (2019) Globally consistent quantitative observations of planktonic ecosystems. *Front. Mar. Sci.*, **6**, 1–16. <https://doi.org/10.3389/fmars.2019.00196>.
- Longhurst, A. R. and Glen Harrison, W. (1989) The biological pump: profiles of plankton production and consumption in the upper ocean. *Prog. Oceanogr.*, **22**, 47–123. [https://doi.org/10.1016/0079-6611\(89\)90010-4](https://doi.org/10.1016/0079-6611(89)90010-4).
- Mansour, J. S., Norlin, A., Llopis Monferrer, N., L'Helguen, S. and Not, F. (2021) Carbon and nitrogen content to biovolume relationships for marine protist of the Rhizaria lineage (Radiolaria and Phaeodaria). *Limnol. Oceanogr.*, **66**, 1703–1717. <https://doi.org/10.1002/lno.11714>.
- McConville, K., Atkinson, A., Fileman, E. S., Spicer, J. I. and Hirst, A. G. (2016) Disentangling the counteracting effects of water content and

- carbon mass on zooplankton growth. *J. Plankton Res.*, **39**, 246–256. <https://doi.org/10.1093/plankt/fbw094>.
- Moriarty, R. and O'Brien, T. (2013) Distribution of mesozooplankton biomass in the global ocean. *Earth Syst. Sci. Data*, **5**, 45–55. <https://doi.org/10.5194/essd-5-45-2013>.
- Motoda, S. (1959) Devices of simple plankton apparatus, 74–91.
- Ohman, M. D. and Romagnan, J.-B. (2016) Nonlinear effects of body size and optical attenuation on diel vertical migration by zooplankton: body size- and light-dependent DVM. *Limnol. Oceanogr.*, **61**, 765–770. <https://doi.org/10.1002/lno.10251>.
- Pesant, S., Not, F., Picheral, M., Kandels-Lewis, S., Le Bescot, N., Gorsky, G., Iudicone, D., Karsenti, E. *et al.* (2015) Open science resources for the discovery and analysis of Tara Oceans data. *Sci. Data*, **2**, 150023. <https://doi.org/10.1038/sdata.2015.23>.
- Petchey, O. L. and Belgrano, A. (2010) Body-size distributions and size-spectra: universal indicators of ecological status? *Biol. Lett.*, **6**, 434–437. <https://doi.org/10.1098/rsbl.2010.0240>.
- Picheral, M., Catalano, C., Brousseau, D., Claustre, H., Coppola, L., Leymarie, E., Coindat, J., Dias, F. *et al.* (2022) The Underwater Vision Profiler 6: an imaging sensor of particle size spectra and plankton, for autonomous and cabled platforms. *Limnol. Oceanogr. Methods*, **20**, 115–129. <https://doi.org/10.1002/lom3.10475>.
- Picheral, M., Guidi, L., Stemann, L., Karl, D. M., Iddaoud, G. and Gorsky, G. (2010) The underwater Vision profiler 5: an advanced instrument for high spatial resolution studies of particle size spectra and zooplankton. *Limnology and Oceanography-Methods*, **8**, 462–473. <https://doi.org/10.4319/lom.2010.8.462>.
- Pinkerton, M. H., Décima, M., Kitchener, J. A., Takahashi, K. T., Robinson, K. V., Stewart, R. and Hosie, G. W. (2020) Zooplankton in the Southern Ocean from the continuous plankton recorder: distributions and long-term change. *Deep-Sea Res. I Oceanogr. Res. Pap.*, **162**, 1–15, 103303. <https://doi.org/10.1016/j.dsr.2020.103303>.
- Platt, T. and Denman, K. (1978) The structure of pelagic marine ecosystems. *J. Cons. Int. Explor. Mer*, **173**, 60–65.
- Remsen, A., Hopkins, T. L. and Samson, S. (2004) What you see is not what you catch: a comparison of concurrently collected net, optical plankton counter, and shadowed image particle profiling evaluation recorder data from the Northeast Gulf of Mexico. *Deep-Sea Research Part I-Oceanographic Research Papers*, **51**, 129–151. <https://doi.org/10.1016/j.dsr.2003.09.008>.
- Romero-Romero, S., Molina-Ramírez, A., Höfer, J. and Acuña, J. L. (2016) Body size-based trophic structure of a deep marine ecosystem. *Ecology*, **97**, 171–181. <https://doi.org/10.1890/15-0234.1>.
- Roullier, F., Berline, L., Guidi, L., Durrieu De Madron, X., Picheral, M., Sciandra, A., Pesant, S. and Stemann, L. (2014) Particle size distribution and estimated carbon flux across the Arabian Sea oxygen minimum zone. *Biogeosciences*, **11**, 4541–4557. <https://doi.org/10.5194/bg-11-4541-2014>.
- Soviadan, Y. D., Benedetti, F., Brandão, M. C., Ayata, S.-D., Irisson, J.-O., Jamet, J. L., Kiko, R., Lombard, F. *et al.* (2022) Patterns of mesozooplankton community composition and vertical fluxes in the global ocean. *Prog. Oceanogr.*, **200**, 1–10, 102717. <https://doi.org/10.1016/j.pocean.2021.102717>.
- Steinberg, D. K. and Landry, M. R. (2017) Zooplankton and the ocean carbon cycle. *Annu. Rev. Mar. Sci.*, **9**, 413–444. <https://doi.org/10.1146/annurev-marine-010814-015924>.
- Stemann, L. and Boss, E. (2012) Plankton and particle size and packaging: from determining optical properties to driving the biological pump. *Annu. Rev. Mar. Sci.*, **4**, 263–290. <https://doi.org/10.1146/annurev-marine-120710-100853>.
- Stemann, L., Eloire, D., Sciandra, A., Jackson, G. A., Guidi, L., Picheral, M. and Gorsky, G. (2008) Volume distribution for particles between 3.5 to 2000  $\mu\text{m}$  in the upper 200 m region of the South Pacific gyre. *Biogeosciences*, **5**, 299–310. <https://doi.org/10.5194/bg-5-299-2008>.
- Turner, J. (2002) Zooplankton fecal pellets, marine snow and sinking phytoplankton blooms. *Aquat. Microb. Ecol.*, **27**, 57–102. <https://doi.org/10.3354/ame027057>.
- Turner, J. (2004) The importance of small planktonic copepods and their roles in pelagic marine food webs, **43**, 255–266.
- Turner, J. T. (2015) Zooplankton fecal pellets, marine snow, phytodetritus and the ocean's biological pump. *Prog. Oceanogr.*, **130**, 205–248. <https://doi.org/10.1016/j.pocean.2014.08.005>.
- Vinogradov and Tseitlin (1983) *The Sea, Volume 8: Deep-Sea Biology*, Harvard University Press, **8**, 217–241.
- Warren, J. D., Stanton, T. K., Benfield, M. C., Wiebe, P. H., Chu, D. and Sutor, M. (2001) In situ measurements of acoustic target strengths of gas-bearing siphonophores. *ICES J. Mar. Sci.*, **58**, 740–749. <https://doi.org/10.1006/jmsc.2001.1047>.
- Wiebe, P. H. and Benfield, M. C. (2003) From the Hensen net toward four-dimensional biological oceanography. *Prog. Oceanogr.*, **56**, 7–136. [https://doi.org/10.1016/S0079-6611\(02\)00140-4](https://doi.org/10.1016/S0079-6611(02)00140-4).
- Yamaguchi, A., Watanabe, Y., Ishida, H., Harimoto, T., Furusawa, K., Suzuki, S., Ishizaka, J., Ikeda, T. *et al.* (2002) Structure and size distribution of plankton communities down to the greater depths in the western North Pacific Ocean. *Deep-Sea Res. II Top. Stud. Oceanogr.*, **49**, 5513–5529. [https://doi.org/10.1016/S0967-0645\(02\)00205-9](https://doi.org/10.1016/S0967-0645(02)00205-9).
- Zhou, M. (2006) What determines the slope of a plankton biomass spectrum? *J. Plankton Res.*, **28**, 437–448. <https://doi.org/10.1093/plankt/fbi119>.